A physically based constitutive model for predicting the surface integrity in machining of Waspaloy

Stano Imbrogno[a,*], Sergio Rinaldi[a], Domenico Umbrello[a], Luigino Filice[a], Rodolfo Franchi[b], Antonio Del Prete[b]

[a]Department of Mechanical, Energy and Management Engineering, University of Calabria, Via P. Bucci, 87036 Rende (CS), Italy

[b]Department of Engineering for Innovation, University of Salento, Via per Monteroni, 73100, Lecce, Italy

*Corresponding author: Department of Mechanical, Energy and Management Engineering, University of Calabria, Via P. Bucci, 87036 Rende (CS), Italy. E-mail address: stano.imbrogno@unical.it, Phone: +39 0984494637.

Abstract

During machining, surface modifications are directly related to the process dynamic affecting the thermo-mechanical properties of the materials. The physics phenomena (such as dynamic recrystallization, hardening and recovery effects) are difficult to be experimentally evaluated during the cutting operations, therefore the simulations are very important tools to understand their evolution. Orthogonal cutting experiments were conducted on Waspaloy under different cutting parameters and lubri-cooling conditions. The machined surfaces were evaluated via optical microscope and the surface integrity was analyzed in terms of microstructural changes and microhardness. The deformation mechanisms that occurred in chip formation and on the machined surface were investigated in order to build-up a physically based constitutive model. Subsequently, the developed material model was implemented via sub-routine in a commercial Finite Element

software. The numerical prediction strategy was validated through comparisons with experimental outcomes (cutting forces, temperature and metallurgical changes) and employed to predict the variables of scientific interest (microstructural modifications and microhardness). The overall absolute error in predicting the principal cutting force, feed force and temperature were approximately equal to 5%, 9% and 7% respectively. Furthermore, the developed model permits to explore the metallurgical changes and their evolution during the machining process varying cutting parameters and lubri-cooling conditions.

Keywords: Material modeling; Waspaloy; machining; surface integrity.

1. Introduction

The aerospace industries have to guarantee extremely high reliability and duration of the manufactured artefacts, consequently, one of the most important topic of research into this sector regards the prediction of the aero-engine component failure. This latter is extremely hard to be estimated, mainly because a complete knowledge of the material changes happening during all the deformation history of the finished product cannot be obtained only via experimental analysis. Moreover, having a deep knowledge of the microstructural behavior of the material under large deformation process, can lead to the improvement of the mechanical properties. This improvement can be achieved optimizing the process parameters and consequently the thermo-mechanical routes of the worked material.

In the manufacturing of jet engines, the components produced by super alloys represent about 50% by weight. This broad contribution is mainly due to their superior mechanical performances under critical working conditions [1-3]. Although they have superior quality, they usually show poor machinability, indeed these materials are also known as “hard-to-cut” materials. Focusing on nickel-based alloys, the Waspaloy is mainly used in jet engines blades and structural components manufacturing thanks to its superior mechanical properties, high oxidation resistance, stiffness and

strength to weight ratio [4]. In last decades, the researches focusing on this material are increasing, mainly because, many efforts are needed to adequately choose the process parameters and lubri-cooling conditions, select the correct tooling, control the machine shop and consequently reduce the work in process [5].

In this context, the numerical simulations lead a significant contribution in improving the product quality by optimization of the manufacturing process parameters, without performing costly experiments. Nowadays the numerical simulation is a very effective approach for gaining also fundamental insight into the evolution of the material microstructure during the metal cutting process. [6, 7].

Generally, in the machining simulation the constitutive material behavior plays an important role in the correct representation of the process. The flow stress is a mathematical description of the relationship between stress and strain on varying physics variables, such as strain-rate and temperature during different deformation mechanisms. Most of the earlier constitutive models, known as phenomenological models, macroscopically describe the material plastic stress-strain response simply fitting the experimental data. This means that the material microstructure and its evolution as well as dislocations density modifications are not included into the model. However, phenomenological models are usually employed to describe the high strain-rate and temperature flow stress response of materials in machining because of easy implementation into the simulation software [8].

A phenomenological model that plays a significant role in FE analysis pf large strains is the Johnson-Cook (JC) model. It is also the most widely used in machining simulations due to its simplicity and because it is defined through simple interpolation of experimental data. This model provides a description of the relationship between true stress and true strain at various strain-rate and temperature, during different deformation mechanisms [9-11]. JC based numerical models can be also coupled with microstructural dependent semi-empirical models, making possible to get information on the surface modifications. Unfortunately, they frequently need to be re-calibrated

considering the various working conditions and the obtained numerical constants have not physical meanings [12-14].

On the other hand, considerable progresses were reached in describing the constitutive relations using dislocation-mechanics based models, particularly for pure metals and alloys. These complex models provide more information on microstructural modifications during the evolution of the material deformation and they consider these effects in the flow behavior [15].

Therefore, they represent a tool to analyze and to understand the effects of the metallurgical micro-scale mechanisms. In particular, these models describe the flow stress of a material as a function of micro-scale phenomena responsible of the strengthening (e.g. interaction between mobile and immobile dislocations) or softening (e.g. dynamic recovery, grain recrystallization or grain boundary sliding).

It is fundamental tenet of materials science that the material thermo-mechanical properties depend on the metallurgical structure and its modifications. In the machining operations, the microstructural evolutions are characterized by the interaction between mobile dislocations and short or long range obstacles (e.g. solute atoms, precipitates, forest dislocations or grain boundaries). In that case, the strengthening or softening phenomena are always governed by strain, strain rate and temperature.

Due to their analytical complexity, the physically based constitutive models have relatively limited application in metal cutting simulation. However, they are more attractive than phenomenological models since they intrinsically permit to simulate all the microstructural changes and understand their evolution during the machining processes, quantifying their effects on the material thermo-mechanical properties. [16, 17].

Many physically based models have been implemented in order to simulate general plastic deformation processes of metals, with different characteristics and applications.

Estrin et al. [18] formulated a discrete dislocation density based model to compute the shear stress in metal deformation, considering two different contributions in dislocation evolution that refers to low dislocation density channels and high dislocation density walls during material deformation.

Based on the same modeling approach, Ding and Shin [19] developed a multi-physics model to simulate the surface microstructure evolution and the hardness changes on the worked surface during machining of AISI 52100 steel.

Lindgren et al. [20] presented a new model based on dislocation density evolution, where the flow stress was assumed to consist of different additive contributions. In detail, this model involved the interaction between the mobile and immobile dislocations, the microstructural effects due to the grain size changes and the short-range interactions of the mobile dislocations with the small particles, as precipitates and small disturbance into the lattice.

The total stress field was computed using the same technique showed by Liu et al. [21], although they differently computed the dislocation density evolution. In fact, the proposed evolution model took into account the hardening and recovery effects on dislocations and their interactions during the plastic deformation.

Concerning Waspaloy, various researches on its mechanical behavior and metallurgical changes were carried out to date. Chamanfar et al. [22] studied the evolution of the flow stress and microstructure at higher temperature performing isothermal compression tests. They proposed a phenomenological material constitutive model. The metallurgical evolution was well investigated, but the material behavior was not affected by the microstructural changes experimentally evaluated. Likewise, Shen et al. [23] performed hot compression tests under different thermo-mechanical conditions, investigating the microstructure modification they discovered different stages of evolutions. They implemented the microstructure model into FE simulations to predict detailed thermo-mechanical histories during forging. However, the material constitutive model did not take into account the microstructure evolution and its effects on the material behavior. In contrast, Del Prete et al. [24] developed a phenomenological constitutive model based on the workpiece initial hardness to simulate the material behavior of the Waspaloy during machining. They validated the model through the prediction of the cutting forces, temperature into the cutting zone and chip morphology. Also Caruso et al. [12] proposed an innovative phenomenological modeling approach

to take into account the microstructural changes effect on the material JC flow stress, implementing the developed model into FE software to simulate the machining process. It is clear by analyzing the literature, that the microstructure and metallurgical changes play an important role on the material behavior and, although several material behavior models have been proposed, these still show poor or missing links between the material modifications and the mechanical properties. Therefore, in order to ensure the designed mechanical properties of the Waspaloy made artifacts, a deeper knowledge of physics correlation between the mechanical behavior and the microstructural evolution under high dynamic loading is required. Thus, the aim of this work are: (i) to investigate the deformation mechanisms of the Waspaloy machined under different lubri-cooling conditions and cutting parameters; (ii) to develop a physically based constitutive model to simulate the material behavior during orthogonal machining; (iii) To develop a Finite Element strategy for numerical prediction of the surface integrity during machining of Waspaloy.

2. Experimental tests

The orthogonal machining tests, under three different lubri-cooling conditions (dry, wet and cryogenic), were conducted on a CNC MAZAK high speed CNC turning center. The experimental plan is reported in Table 1 and they consisted in radial facing operations of Waspaloy (45 HRC) disks at different cutting speeds and feed rate. Tests were performed using S quality rhomboidal 55° coated carbide tool, mounted on a DDJNR 2525M 15 tool holder (provided by Sandvik Coromant©). This latter was fixed on a piezoelectric dynamometer (Kistler© 9257), in order to measure the cutting forces. Temperatures on the tool-chip interface were also measured during the machining tests via IR thermo-camera provided by FLIR (A6000-series). Further details about the experimental trials are described in a previous work [4]. Finally, all the samples were sectioned, mounted, polished and etched to carry out metallographic and microhardness analysis. The etchant employed was the Kalling's reagent that is recommended for aged and solution treated material. The microstructure of the worked samples was analyzed using optical microscope (Leica© DFC320

1000x). The microhardness ($HV_{0.01}$) was measured on polished samples using a QNES 10 micro-indenter for 10s of pause time.

3. Deformation mechanism

Generally, during machining processes, the material is subjected to severe plastic deformation and the interested regions are both the surface-subsurface zone and the chip. The metallurgical phenomena induced by the tool action are usually characterized by strongly deformed grains (shape modification), changes in dislocation density and their accumulation region, grain refinement (dynamic recrystallization that lead to new microstructures formation) as well as precipitation and phases modifications [25, 26]. The nickel-based super alloys, when subjected to machining operations, usually show recrystallized, highly deformed region within the grains and different altered layers with varying intensity of deformation in surface and subsurface of the worked material. In detail, normally the affected layer shows the generation of slip band, grains elongation in the cutting direction, white layer formation and dynamic recrystallization due to the thermo-mechanical loads induced by manufacturing processes [1, 26]. Concerning the investigated Waspaloy, a schematic representation of the different metallurgical phenomena induced by different rate of plastic deformations is represented by Figure 1. Figure 1(a) is representative of the machined material cross section. The strongly deformed grains were isolated and the different deformation mechanisms were investigated (Figure 1(b), 1(c) and 1(d)). At lower aggressive machining conditions (low feed rate and cutting speed) the main deformation mechanism that characterize the microstructure is represented by Figure 1(b). The grains subjected to plastic deformation show wide regions of slip band concentrations. The glide of many dislocations, resulting in slip bands, is the most common manifestation of plastic deformation in crystalline solids, resulting in the increasing of the material strength (strain-hardening). Their presence represents the paths of dislocations during movement, that happens in the direction where the atoms are most closely spaced [27]. When the strain and strain rate increase (corresponding in the increasing of the cutting speed and

feed rate), the slip bands start to form cell structures due to the double-cross slip mechanism. This effect leads to the growth of slip bands by the sidewise spreading of slip, as shown in Figure 1(c). The double-cross slip events of smaller height may lead to multiplication at higher stresses, while the slip bands tend to become narrower at low temperatures [28, 29]. When machining conditions became aggressive, then sub-micron grains with sharp boundaries are formed in severer deformation conditions, via reorganization of the dislocations within the dislocation cells (Figure 1(d)) and some grains start to recrystallize [30], resulting in material strengthening due to Hall-Petch effect [31].

The different deformation mechanisms described before are visible in the machined chip and both in machined surface and sub-surface (Figure 2).

In serrated chip, two different deformation mechanisms are visible in two insulated zones identified as the Low Shear Strain Zone (LSSZ) and the High Shear Strain Zone (HSSZ). In LSSZ, that is far from shear band, the microstructure showed poor deformation and the grains had almost the same size of the as-received microstructure (Figure 2a). In HSSZ, that is within the shear band, it was possible to observe elongated grain structures and grain refinement due to the extremely large deformations (Figure 2b). Analyzing the microstructure of the machined surface, it is possible to notice that all the previously explained deformation mechanisms are clearly visible. Indeed, in the region very close to the worked surface the grain refinement is quite appreciable (Figure 2c). This result was very highlighted when severer cutting conditions were adopted. Generally, the highly deformed microstructure was always present in each sample (Figure 2d). From the worked surface to the depth, the effects of the large deformations fade away, showing slight deformation effects (Figure 2e) in the sub-surface and undeformed microstructure distant from the machined surface (Figure 2f).

4. Physically based constitutive model

The real description of the material behavior in terms of true stress-true strain represents a key role for understanding the reasons of the mechanical response of the manufactured components under different strain, strain rate and temperature conditions. The physical based models are preferred because they can catch the natural phenomena dominating the deformation based on the physics events coupled with the microstructure evolution [27]. In this work, a physically based plasticity model for Waspaloy has been developed and implemented in machining simulation. The macroscopic flow stress is assumed to consist of additive long-range and short-range contributions (Equation 1).

$$\sigma = \sigma^* + \sigma_G + \sigma_{HP} \quad (1)$$

where σ^* is representative of the short-range contribution and is thermally activated. It is the stress needed for a dislocation to pass short-range obstacles and to move it through the lattice. The thermal vibrations can assist the stress to overcome these obstacles. σ_G denotes the long-range and it is often called strain hardening due to the forest dislocations, σ_{HP} is the Hall-Petch (i.e. grain size contribution to the flow stress). The long-range contribution are sometimes considered as athermal contribution because the thermal vibrations cannot assist a moving dislocation to pass the region subjected to long-range distortion of lattice [32].

4.1 Long-range contribution - strain hardening

The interaction between moving dislocations and immobile dislocations is a long-range interaction (if it cuts orthogonal to the dislocation is of short-range). This interaction is the physical basis of the strain-hardening of a metal. The long-range contribution to the material resistance is represented by Equation 2 (σ_G). This mechanical resistence is due to the interactions with the dislocation substructure [33].

$$\sigma_G = M\alpha Gb\sqrt{\rho_i} \quad (2)$$

In Equation 2, α is a proportional constant, M is the Taylor factor, ρ_i is the density of immobile dislocations and G is the temperature dependent shear modulus, b is the Burger's vector (2.50e-10m [34]).

The immobile dislocation density evolution is described by Equation 3 (density dislocation evolution) [35, 36]. The evolution equation consists of two terms: $\dot{\rho}_i^{(+)}$ that is representative of the hardening and $\dot{\rho}_i^{(-)}$ that is representative of the softening due to the recovery.

$$\dot{\rho}_i = \dot{\rho}_i^{(+)} - \dot{\rho}_i^{(-)} \tag{3}$$

4.2 Hardening contribution

The mobile dislocations may encounter obstacles that prevent further movement and as a result become immobilized due to the trapping effect of the obstacles. Moreover, when dislocations are moving next to the grain boundaries can be annihilated due to the interactions with dislocations of opposite sign. The increase in dislocation density is assumed to be proportional to the plastic strain rate [37, 38].

$$\dot{\rho}_i^{(+)} = \left(\frac{1}{s} + \frac{1}{D}\right)\frac{M}{b}\dot{\varepsilon}^p = \frac{M}{b\Lambda}\dot{\varepsilon}^p \tag{4}$$

Where $\dot{\varepsilon}^p$ is the equivalent plastic strain rate and Λ interprets the mean free path of a moving dislocation until it is immobilized. In the Equation (4), D and s represents the grain size and the cell size respectively. The cell size is assumed to be inversely proportional to the square root of the immobile dislocation according to Equation 5 [39].

$$s = K_c/\sqrt{\rho_i} \tag{5}$$

where K_c is a calibration parameter.

4.3 Softening contribution

Different processes may contribute to the reduction of the dislocation density. They are separated into static and dynamic recovery as:

$$\dot{\rho}_i^{(-)} = \dot{\rho}_{sr}^{(-)} + \dot{\rho}_{dr}^{(-)} \tag{6}$$

The $\dot{\rho}_{sr}^{(-)}$ represents the static recovery. This formulation is depending on some physics constants as Boltzmann's constant (k_b) and self-diffusivity models. It is also depending on grown of dislocation density that is used in the model to prevent that the dislocation density become zero when very long times are considered in the process. In the machining simulation, a very short interval time proportional to 1e-7s is considered, consequently its contribution ($\dot{\rho}_{sr}^{(-)}$) was neglected. On the contrary, the dynamic recovery terms is proportional to the immobile dislocation density and the plastic strain rate (Equation 7). The dynamic recovery implies that moving dislocation annihilates the immobile ones.

$$\dot{\rho}_{dr}^{(-)} = \Omega \rho_i \dot{\bar{\varepsilon}}^p \tag{7}$$

where Ω is a recovery function and its expression is reported in Equation 8

$$\Omega = \Omega_0 + \Omega_{r0} \left(\frac{1}{\dot{\bar{\varepsilon}}^p} \frac{D_v}{b^2} \right)^{1/3} \tag{8}$$

$$D_v = D_{v0} exp(-Q_v / k_b T) \tag{9}$$

Where D_v (Equation 9) is a diffusivity, while Ω_0 and Ω_{r0} are two calibration parameters, D_{v0} is a numerical constant, Q_v is the activation energy for self-diffusion. As reported in literature, the recovery for the dislocations takes place mainly in the cell walls and this process is due to climb controlled by excess vacancies created during deformation [35-37, 40].

4.4 Hall-Petch effect

The Hall-Petch effect is due to the resistance to dislocation motion offered by grain boundaries. In detail, this effect is due to the pile-up of dislocations at grain boundaries leading to the activation of

other slip systems in the surrounding grains [41]. The representative model of the Hall-Petch contribution to the flow stress is computed as showed by Equation 10:

$$\sigma_{HP} = k_{HP}/\sqrt{D} \tag{10}$$

Where D is the grains size. As grains are refined progressively, once they decrease under a critical value the material strength starts to decrease. This phenomenon is commonly referred to the inverse Hall-Petch effect and different physical explanations are available in literature [42-46]. The coefficient k_{HP} catches this physics phenomenon that is particularly evident (Figure 1 and Figure 2) as a grain boundary sliding coupled with significant grain refinement. This results in a softening effect on the material constitutive behavior and this effect is captured by the Equation 11 [47]:

$$k_{HP} = \alpha_G^0 tanh\left(\frac{d}{D^{-0.5}}\right)^{\nu} \tag{11}$$

Where α_G^0, d and ν are calibration parameters, D is the grain size due to continuous grain refinements.

4.5 Grain size evolution

The grain size D has been computed taking into account the common mixture law (Equation 12):

$$D = D_{DRX}X_{DRX} + D_0(1 - X_{DRX}) \tag{12}$$

Where D_0 is the average initial grain size (41 μm), X_{DRX} is the volume of the recrystallized microstructure and is represented by the Avrami model asserting that the DRX has a sigmoidal evolution showed by Equation 13. It depends on strain ε, while ε_{cr} is the critical strain for the nucleation of the recrystallized grains (Equation 13) and $\varepsilon_{0.5}$ (Equation 15) that is the strain referred to the 50% of recrystallized microstructure. Generally, the ε_{cr} is equal to the $0.8\varepsilon_{peak}$ (Equation 14) that denotes the strain corresponding to the maximum stress. The D_{DRX} is the dynamically recrystallized grain size computed as shown by Equation 16. The D_{DRX} is a function of two material

constants and the Zener-Hollomon parameter (Equation 17). The constant R in Equation 17 is the universal gas constant.

$$X_{DRX} = 1 - exp\left(-\log 2\left(\frac{\varepsilon-\varepsilon_{cr}}{\varepsilon_{0.5}}\right)^3\right) \quad (13)$$

$$\varepsilon_{peak} = 5.375 \cdot 10^{-4} {D_0}^{0.54} Z^{0.106} \quad (14)$$

$$\varepsilon_{0.5} = 0.1449 {D_0}^{0.32} Z^{0.03} \quad (15)$$

$$D_{DRX} = 8103 Z^{-0.16} \quad (16)$$

$$Z = \dot{\varepsilon}^p exp\left(\frac{468000}{RT}\right) \quad (17)$$

The Equations from 13 to 17 are reported in [23] and [48] and are referred to the microstructural evolution during thermo-mechanical operation under temperature lower than 1010 °C. As a matter of fact, no thermal gradient greater than 750 °C were reached during the experimental cutting tests and this result justifies the decision to choose these set of equations although in the work of Shen et al. [23] are developed the equations for higher temperatures as well.

4.6 Short-range contribution

The σ^* term represents the material resistance to plastic deformation due to the short-range interactions where thermal activated mechanisms assist the applied stress in moving dislocations (Equation 18). Short-range obstacles are a general classification of any disturbance of the lattice that is 'small enough' so that thermal vibrations can, together with the effective stress, move the affected part of a dislocation through that region [49].

$$\sigma^* = \sigma_0\left(1 - \left(\frac{k_b T}{\Delta f_0 G b^3} ln\left(\frac{\dot{\varepsilon}_{ref}}{\dot{\varepsilon}^p}\right)\right)^{1/q}\right)^{1/p} \quad (18)$$

where k_b is the Boltzmann constant, T is the temperature, Δf_0 , q and p are calibration parameter and $\dot{\varepsilon}_{ref}$ is typically taken as 10^6 or 10^{11} [50], σ_0 is the frictional stress and its value is equal to 683MPa [34] .

4.7 Hardness prediction model

The strengthening induced by the machining operation on the material can be modeled as suggested by Equation 19:

$$\Delta h = k_h M \alpha G b \sqrt{\rho_i} \tag{19}$$

this model has been successfully implemented via sub-routine by Ding and Shin [51]. k_h is a material constant that has been calibrated taking into account the experimental results. The obtained value was equal to 80.18 in order to compute the resulting hardness in Vickers. In Figure 3 is reported the prediction strategy implemented by sub-routine into the FE software SFTC DEFORM© in order to simulate the constitutive material behavior of the Waspaloy during machining operations.

To obtain the correct value of the numerical constants of the material behavior developed model, a fitting procedure of experimental true stress-true strain has been carried out. The calibration procedure was stopped when the error between the predicted and the experimental flow stress was minimized. The value of the obtained calibrated constants or obtained by literature analysis are reported in Table 2.

5. Finite Element Model

A Finite Element physics-based model of the orthogonal cutting process has been developed using the commercial software SFTC Deform 2D®. A plane-strain thermo-mechanical analysis was performed via Update-Lagrangian code with remeshing technique.

The workpiece was meshed with 20000 isoparametric quadrilateral elements, with a severe mesh refining near the cutting zone, having here a mean element size of 2μm, in order to obtain more accurate results on the worked surface and a better chip geometry. The tool has been modelled in the FE software as a rigid body and the geometry has been obtained studying the cutting tool using a ConScan Surface Profilometer Anton-Paar. In detail, the tool was scanned by a laser on the section transversal to the cutting direction and the obtained profile was imported into the FE software. The interaction between the tool and the workpiece was modelled by implementing the hybrid friction model in order to take into account both the effects of sticking and sliding at tool-chip interface. Considering the thermal aspects of the model, the global heat transfer coefficient (h_{int}) at the tool-workpiece interface was set equal to 10^5 kW/(m^{2}K) according to the guidelines and literature results [7, 8]. Concerning the machining tests under wet and cryogenic lubri-cooling condition, to better simulate the two different cooling effects more consideration had to be done than dry cutting simulations. In detail, an environmental window for heat exchange have been considered and two different values for the heat transfer coefficient (h_{local}) has been set at the tool-chip interface. The value of h_{local} has been calculated using Equation 20, according with [52].

$$h_{local} = \frac{0.20}{e^{0.35} g^{0.33}} \frac{{V_f}^{0.65} {k_f}^{0.67} {c_p}^{0.33} {\gamma_f}^{0.33}}{{\nu_f}^{0.32}} \quad (20)$$

Where e is the equivalent length and g is the gravitational acceleration, while the remaining parameters are related to the cutting fluid: V_f is the velocity, k_f is the thermal conductivity, γ_f is the specific weight, $\boldsymbol{\nu}_f$ is the dynamic viscosity and c_p is the specific heat capacity of the lubri-coolant fluid considered. In this specific case, the equivalent length was referred to the diameter of the nozzle.

5.1 Friction Model Calibration and Validation

The friction model employed in machining simulations was the hybrid model, it is particularly suited to simulate machining operations [7, 12, 13, 24]. This model depends on two coefficients (μ and m) and singularly describes the effects of sticking and sliding conditions that happen at the tool-chip interface. The aim of the calibration phase was to obtain the numerical value of the friction coefficients on varying cutting speed and feed rate. The values of the coefficients were determined through an iterative calibration strategy based on classical "trial and error" technique. Particularly, it consisted to compare the experimental cutting forces and temperatures with those predicted, modifying the friction coefficients until the error did not reach value lower than 10%. The calibration was carried out by FE analysis considering various cutting speeds and feed rates for each individual lubri-cooling condition and interpolating the obtained coefficients values through Response Surface Optimization Methodology (RSM) using MATLAB© curve fitting tool. These values, visible in Table 3, represent the results of the best trade-off regarding the absolute error between the considered variables (cutting forces and temperatures).

In the calibration phase, it was necessary to employ four proper case studies among the experimental test, because it is the minimum number suggested by the software that allows to develop the friction equations as a bi-linear law. The RSM permitted to obtain the previously reported models with very high predictive capacity, having a coefficient of determination R^2 very close to 1. Once the coefficient were calibrated, the FE model has been validated by comparing the experimental data with the other corresponding simulation results and the results are reported in Table 4. The predicted principal cutting forces were in a good agreement with the ones found in the experiments, with an overall average error of 4.76%. The predicted feed forces showed a total absolute error equal to 9.21%, that was higher than the principal cutting force. However, due to the very complex deformation process simulated, this specific entity of error was considered acceptable. Moreover, it is important to highlight that the tool geometry changes due to the wear. This aspect was not modelled because of higher computational time caused by a significant number of equations involved. Therefore, the higher error in feed force was also attributed to the absence of

tool wear in the finite element model, which was unavoidably present in the machining processes of super alloys [4, 47]. Concerning the temperature into the cutting zone was successfully predicted with an overall average error of 6.97%. This suggest that the developed thermo-mechanical numerical strategy was correctly modelled.

At the end of the calibration, the equations describing the trends of the friction coefficients μ and m, were defined dependent on the cutting parameters (cutting speed V_c and feed rate f), as illustrated in Equations (21) and (22) for dry condition, (23) and (24) for wet condition, (25) and (26) for cryogenic condition:

$$\mu(V_c, f)_{DRY} = 0.5567 - 0.00227 * V_c - 1.213 * f \quad (21)$$

$$m(V_c, f)_{DRY} = 0.5881 - 0.00581 * V_c + 0.3048 * f \quad (22)$$

$$\mu(V_c, f)_{WET} = -0.04 + 0.000222 * V_c + 2.2 * f \quad (23)$$

$$m(V_c, f)_{WET} = -0.04 + 0.000222 * V_c + 2.2 * f \quad (24)$$

$$\mu(V_c, f)_{CRYO} = 0.5306 - 0.00278 * V_c - f \quad (25)$$

$$m(V_c, f)_{CRYO} = 0.5306 - 0.00278 * V_c - f \quad (26)$$

Taking into account the friction coefficient values showed in Table 3 and in Table 4, generally, they show a decreasing trend with the increase of the cutting speed. Considering dry and cryogenic machining conditions, the coefficients tend to maintain slightly different value, in good agreement with the results found by Courbon et al. [53]. On the other hand, the usage of the lubri-coolant in wet conditions gravely reduces the friction effects and so the values of the coefficients.

The numerical values of the predicted variables (cutting and feed forces and temperatures) compared with the experimental ones are also reported in Figure 4 for dry cutting condition, in Figure 5 for wet cutting condition and in Figure 6 for cryogenic condition

As previously explained in Section 3, during the chip serration formation it is possible to observe both HSSZ and LSSZ due to the competition of strain hardening and thermal softening phenomena. This experimental evidence was also successfully predicted, as shown in Figure 7, Figure 8 and Figure 9 in dry, wet and cryogenic machining conditions respectively. Taking into account the micrographs, the deformed region changes its morphology depending on the cutting parameters and cooling conditions. The HSSZ was characterized by strong deformed grains with severe modifications of substructures, while in LSSZ was possible to see that grains were slightly deformed or in the cases that showed a strongly serrated chip, grains were very similar to material not deformed (e.g. V_c= 40 m/min, f = 0.15 mm/rev – dry condition). The chip predicted by the numerical model showed a low strain value exactly in the LSSZ while higher values of plastic deformation were reached into the thin shear zone (HSSZ).

It is also important to highlight that the occurrence of segmentation, as well as almost continuous chip formation at varying cutting parameters and cooling conditions was predicted by the model. As suggested by Umbrello [54], a good measure of the accuracy of a machining numerical model is also suggested by its capability to correctly predict the chip formation during the machining process, this statement suggests the excellent robustness of the proposed numerical model.

6. Surface integrity analysis: results and discussion

The thermo-mechanical loads induced by machining process caused substantial microstructural modifications on the worked surface [25]. The trigger and the evolution of these microstructural changes is extremely hard to be evaluated via experimental analysis, but the physics based FE model allows to have a complete assessment of these phenomena while they start and evolve during the machining process.

The microstructural modifications experimentally observed were deeply investigated through the numerical model once the validation phase was completed. In particular, they usually consisted of large deformed grains; but depending on the cutting speeds, feed rate and cooling conditions,

further dynamic phenomena usually occurred. Beneath the worked surface, it was possible to observe plastically deformed grains characterized by diffused intersecting slip bands due to the localized shear effects. The slip bands behave as preferred site for development of highly misoriented structures [55]. These phenomena were more evident in HSSZ of the chip microstructure, where plastic deformation was extremely higher. Huang and Logé [56] described the metallurgical phenomena that happens into the strongly deformed region, where it was possible to relief a high concentration of dislocations arranged into cellular substructures, which generally are considered as preferred grains nucleation zones, causing DRX phenomena.

In detail, in Figure 10 and Figure 11 are reported the comparison of the micrographs and the numerical results of the altered microstructure on the machined surface and the chip.

The FE simulation was able to easily predict the grain size changes due to the thermo-mechanical load induced by cutting into the chip as well as on the machined surface. Although, the high refinement made difficult the experimental quantitative analysis of the microstructure into the shear band and in the ultrafine grain layers beneath the machined surface, the numerical model showed a reliable predictive capability related to these phenomena. It is important to highlight that the model was able to predict not only the new grains formation and evolution, but also the dimension of the region characterized by the severe grains refinement (altered layer thickness beneath the machined surface). In detail, taking into account the Figure 10, the optical micrograph showed a thin homogeneous layer (almost 8μm) in which the grains were very small and thus it was difficult to quantify their dimensions. The comparison with the numerical prediction suggested that the very thin layer was mainly characterized by very small grains with dimensions lower than 4μm difficult to be caught by optical microscopy. Moreover, the dimension of the affected layer predicted was perfectly comparable with the experimental one; therefore, the numerical developed model was able to predict the thickness of the altered material. The very good numerical results were also obtained changing cutting parameters and cooling strategy. The reason of the grain refinement, as suggested by the numerical prediction strategy, was due to the dynamic phenomena as DRX. Therefore, based

on the FE model outcomes, it is possible to claim that dynamically recrystallized grains mainly characterize the very thin layer. This latter was mainly experimentally observed in the case studied where the cutting parameters were critical (V_c=70m/min, f=0.15mm/rev) under cryogenic conditions. These ultrafine grain layers were less evident on the samples machined under dry conditions while the wet conditions totally avoided this kind of phenomenon. The presence of dynamically recrystallized grains particularly promoted by the cryogenic environment during machining processes was extensively investigated and confirmed from many researchers [1, 57, 58]. Indeed, the cryogenic fluid immediately freezes the very hot material into the cutting zone totally avoiding any grain growth and recovery effect. The physics based model showed the ultrafine grain layer formation due to DRX only when the cryogenic machining was simulated. Indeed, the thermal conditions that modelled the presence of liquid nitrogen were set through environmental windows into the cutting zone, while to simulate the dry conditions, only the exchange heat with the environment was used due to the lack of lubri-coolants. Therefore, it is clear that the thermal conditions also play an important role in inducing microstructural changes. The capability of the cryogenic machining to promote the DRX and avoid the recovery phenomena is well assessed by the scientific community [59] and this aspect is well represented by the FE model. Therefore, the developed strategy can be effectively used to understand the reason of the thin layer formation, its composition, the microstructure size and its evolution depending on the cutting parameters and cooling conditions.

In Figure 11 is reported the comparison between the numerical and experimental microstructural alteration due to the cutting operation within the chip. As previously mentioned in Section 3, the serrated chip was characterized by two regions with different microstructural features. The experimental observation did not permit to deeply know the metallurgical phenomena that occurred into the HSSZ as well as their evolution at vary thermo-mechanical loads. However, the FE developed strategy allowed to study the occurrence of the new microstructures. As showed by the simulated chip formation, the grain size inside the HSSZ was finer than the surrounded one (usually

slightly deformed) and the dynamic phenomenon that leads to the grain refinement was the DRX due to the combination of high temperature and plastic deformation. The new microstructure consisted of sub-micrometer grains according with the results reported by Ni and Alpas [30], Fernandez-Zelaia [60] and Ravi Shankar [61, 62]. Moreover, the width of the deformed and undeformed zones were clearly distinguishable thanks to the grain size changes (Figure 11) and were completely comparable with the optical micrograph.

It is well known that the tool action on the machined surface typically causes material changes and consequently modification of the material properties. Generally, large plastic deformations lead to work hardening phenomenon that is usually experimentally appreciated by hardness measurements. The hardness variation is commonly attributed by the grain size changes and is analytically described by the Hall-Petch equation [20]. However, the regions beneath the machined surface, where the measured hardness showed higher variations, were wider than the layers characterized by DRX (Figure 12). These results suggest that the DRX was not the main responsible of hardness increasing, indeed below the DRX layer the grains showed regions subjected to substantial slip activities that means increment of dislocation density [63]. Consequently, the numerical model was useful to investigate the role of dislocations in relation with the hardening and recovery phenomena. It is important to highlight that the dislocation density computed on sub-surface were more concentrated in the region experimentally characterized by slip bands. Moreover, the accumulation of dislocations led to hardness variation as predicted by the model, and the results are in agreement with the measurements (Figure 12). The overall comparison between the experimental and numerical hardness value is showed by Figure 13. The data were collected in all the analyzed cases on the worked subsurface starting from a depth of 15μm. It is possible to observe (Figure 13a, 13b and 13c) that the developed model was able to predict the hardness at varying cutting speed, feed rate and cooling conditions. This latter also supported the right modeling strategy used to take into account the cooling phenomenon. The maximum average error between the numerical and experimental results did not exceed the 5%. Moreover, as suggested by Figure 14, the robustness of

the model was also confirmed by the hardness prediction through the entire affected layer. This very good result is highlighted in Figure 14a, 14b and 14c at various cooling conditions. It is important to point out that the good prediction of the hardness variation by the FE model permitted to better evaluate the affected layer thickness.

7. Finite Element Analysis

The FE simulation allowed to predict the cutting forces and temperature as well as to identify the grain size modification range, their related formation mechanism, the dislocations accumulation and their effect on the hardness beneath the machined surface. In detail, as previously mentioned in paragraph 6, the combination of higher cutting parameters (V_c=70m/min, f=0.15mm/rev) and the cryogenic fluids led to formation of ultrafine grain layers. These phenomena were less evident on the samples machined under dry conditions while they were never observed under wet machining conditions. The reliability of the model in predicting fundamental variables (cutting forces and temperatures) as well as metallurgical changes were validated; therefore, the developed model can be used to explore the effects of further cutting parameters on the machined surface. Generally, the increment of the cutting speed permits to reduce the manufacturing time leading to an improvement of the overall production, thanks to the developed model it is possible to anticipate the cutting forces, temperatures and surface integrity and thus the global feasibility of the process parameters selected. Therefore, the authors decided to perform a Finite Element Analysis (FEA) increasing the cutting speed to 85m/min keeping the feed rate at two levels (0.05mm/rev and 0.1mm/rev) and considering the same cooling strategies (dry, wet and cryogenic). It is important to highlight that the feed rate equal to 0.15mm/rev was not included in the analysis since the experimental results showed intense tool wear and a catastrophic tool failure during dry tests at the studied cutting speeds (55m/min and 70m/min) [4]. As showed in Figure 15 (a), 15 (b) and 15 (c), the feed rate and the cooling conditions affect the cutting forces and the temperature. Generally, increasing the

cutting speed from 70m/min to 85m/min with fixed feed rate of 0.05mm/rev the main cutting and thrust forces slightly decrease of 3% while at feed rate of 0.1mm/rev the decrease is equal to 5%. It is possible to claim that the cutting forces variation is almost negligible and the trend reached a steady state. However, at high cutting speed (85m/min) the difference is still evident at different feed rate and cooling conditions. The lower temperatures produced by the cryogenic fluid led to higher cutting and thrust forces compared to wet and dry conditions. Concerning the metallurgical phenomena, the higher cutting speed led to smaller grains formation due to dynamic recrystallization, indeed the combination of thermo-mechanical load triggered the nucleation and formation of new grains. Regardless the cooling conditions, the formation of larger recrystallized grains induced by a machining operation with cutting speed of 85m/min respect to the ones obtained at cutting speed of 70m/min was mainly due to the higher cutting temperatures. On the other hand, a different situation appeared taking into account the dislocations accumulation and thus the hardness on the machined surface. Focusing at 15μm beneath the machined surface, then excluding the recrystallized region, the dislocations density, the plastic deformation and subsequently the hardness were computed depending on the cutting speed (70m/min, 85m/min), feed rate (0.05mm/rev. 0.1mm/rev) and cooling strategy (dry, wet and cryogenic) (Figure 16 and Figure 17). Considering the feed rate of 0.05mm/rev, the increase of the cutting speed from 70m/min to 85m/min led to the increase of plastic deformations and temperature on the machine surface. However, the plastic deformation had a predominant effect promoting the dislocations accumulation and thus the raise of hardness. As showed by Figure 17 (a), the material exhibited a strain hardening behaviour under dry, wet and cryogenic. On the contrary, at higher feed rate (0.1mm/rev), the increase of cutting speed led to an increase of cutting temperature and consequently a lower accumulation of plastic deformation (dry and wet conditions) causing a decrease of dislocation densities and thus of hardness (Figure 16 a and Figure 17 b). Taking into account dry and wet conditions, it is possible to observe that despite the plastic strain at higher cutting speed was lower, the cryogenic machining still permitted to reach higher plastic

deformations. However, the difference of temperature at feed rate of 0.1mm/rev was more significant (60 °C) than the one observed at lower feed rate (23 °C), therefore the higher thermal gradient led to a predominant thermal softening effect against the higher plastic strain under cryogenic conditions. Moreover, the higher temperature difference under cryogenic machining led to a lower accumulation of dislocations due to the predominance of recovery (Figure 17 b). This analysis highlights that machining Waspaloy with cutting speed higher than 70m/min does not permit to achieve higher hardness values beneath the machined surface without correctly setting the feed rate parameter. The FEA showed an upper limit in improving the surface integrity in terms of hardness, in fact, as showed by Figure 17 (b), the cooling strategy did not significantly affect the dislocation density and thus the hardness, but the most relevant variation was due to the cutting speed once the feed rate exceeded the value of 0.05mm/rev.

7. Conclusions

In this study the metallurgical phenomena induced by orthogonal cutting on Waspaloy was experimentally investigated and numerically modelled. The main deformation mechanisms that affect the material during plastic deformation were preliminarily studied. The nickel-based super alloy analysed showed significant plastically deformed regions characterized by grains with altered shapes, intense slip activity and in some cases recrystallization depending on the thermo-mechanical loads. Subsequently, a proper physics based modeling approach was developed to model the previous mechanisms identified and to study the metallurgical phenomena that were hard to be experimentally investigated. The reliability of the FE strategy was confirmed by the good prediction of the variables of industrial interest, i.e. cutting forces and temperatures at the contact surface between the worked material and the cutting tool. Furthermore, the model predicted the metallurgical micro-scale and nano-scale phenomena on the chip and on the machined surface and sub-surface, as grain refinement layers and dislocation accumulation on the strongly deformed

regions. In detail, the appearance of very thin layers of deformed material characterized by very small and indiscernible grains was numerically analyzed via FE simulations. The obtained results evidenced the new grain formations (sub-micrometer dimension) as dynamic recrystallization phenomenon due to the combination of very large strains and rapid freezing of the machined surface. Furthermore, the hardness variation induced by machining operation was experimentally measured. This variation was observed in a larger region characterized especially by deformed grains subjected to intense slip activity instead of grain refinement. In detail, in these regions the FE model predicted the hardening effect due to the accumulation of dislocations where dynamic recrystallization did not also occur. Subsequently a FEA was performed to study the effect of higher cutting speed, namely 85m/min, on the cutting forces, temperature and surface integrity. The FEA showed that when the feed rate was fixed to 0.05mm/rev, the Waspaloy showed a strain hardening effect predominant when the cutting speed was increased while at higher feed rate (0.1mm/rev) the higher cutting speed led to thermal softening effect predominant. This latter led to recovery effect, less accumulation of dislocation and thus sub-surface hardness. Finally, the model can be used to easily study the complex metallurgical phenomena that occur during machining operation performed on Waspaloy under different lubri-cooling conditions and cutting parameters.

References

[1] A. Thakur, S. Gangopadhyay, State-of-the-art in surface integrity in machining of nickel-based super alloys, Int. J. Mach. Tools Manuf. 100 (2016) 25-54.

[2] H. S. Mali, D. R. Unune, Machinability of Nickel-Based Superalloys: An Overview, Reference Module in Materials Science and Materials Engineering (2017), https://doi.org/10.1016/B978-0-12-803581-8.09817-9.

[3] S. Birosca, F. Di Gioacchino, S. Stekovic, M. Hardy, A quantitative approach to study the effect of local texture and heterogeneous plastic strain on the deformation micromechanism in RR1000 nickel-based superalloy, Acta Mater. 74 (2014) 110–124.

[4] S. Rinaldi, S. Caruso, D. Umbrello, L. Filice, R. Franchi, A. Del Prete, Machinability of Waspaloy under different cutting and lubri-cooling conditions, Int. J. Adv. Manuf. Technol. 94 (2018) 3703–3712.

[5] P. J. Liew, A. Shaaroni, N. A. C. Sidik, J. Yan, An overview of current status of cutting fluids and cooling techniques of turning hard steel, International Journal of Heat and Mass Transfer 114, (2017) 380-394.

[6] İ. Ucun, K. Aslantas, Numerical simulation of orthogonal machining process using multilayer and single-layer coated tools, Int J Adv Manuf Technol 54 (2011) 899–910.

[7] P. J. Arrazola, T. Özel, D. Umbrello, M. Davies, I. S. Jawahir, Recent advances in modelling of metal machining processes, CIRP Ann-Manuf. Technol. 62 (2013) 695-718.

[8] S. N. Melkote, W. Grzesik, J. Outeiro, J. Rech, V. Schulze, H. Attia, P. J. Arrazola, R. M'Saoubi, C. Saldana, Advances in material and friction data for modelling of metal machining, CIRP Ann-Manuf. Technol. 66 (2017) 731-754.

[9] G. R. Johnson, W.H. Cook, A constitutive model and data for metals subjected to large strains, high strain rates and high temperatures. Proceedings of the 7th International Symposium on Ballistics, 54 (1983) 1-7.

[10] A. Dorogoy, D. Rittel, Determination of the Johnson–Cook Material Parameters Using the SCS Specimen Exp. Mech. 49 (2009) 881–885.

[11] F. Karaa, K. Aslantas¸, A. Çiçek, Prediction of cutting temperature in orthogonal machining of AISI 316L using artificial neural network, Applied Soft Computing 38 (2016) 64–74.

[12] S. Caruso, S. Imbrogno, S. Rinaldi, D. Umbrello, Finite element modeling of microstructural changes in Waspaloy dry machining, Int. J. Adv. Manuf. Technol. 89 (2017) 227-240.

[13] F. Jafarian, M. Imaz Ciaran, D. Umbrello, P. J. Arrazola, L. Filice, H. Amirabadi, Finite element simulation of machining Inconel 718 alloy including microstructure changes, Int. J. Mech. Sci. 88 (2014) 110-121.

[14] J. Yanagimoto, K. Karhausen, Incremental Formulation for the Prediction of Flow Stress and Microstructural Change in Hot Forming, J. Manuf. Sci. Eng. 120 (1998) 316-322.

[15] F. J. Zerilli, R.W. Armstrong, Dislocation-Mechanics-Based constitutive relations for material dynamics calculations, J. Appl. Phys. 61 (1987) 1816-1825.

[16] H. Mecking, U. F. Kocks, Kinetics of flow and strain-hardening, Acta Metall. 29 (1981) 1865-1875.

[17] G. Girardin, C. Huvier, D. Delafosse and X. Feaugasa, Correlation between dislocation organization and slip bands: TEM and AFM investigations in hydrogen-containing nickel and nickel–chromium, Acta Mater. 91 (2015) 141–151.

[18] Y. Estrin, L. S. Tòth, A. Molinari, Y. Bréchet, A dislocation-based model for all hardening stages in large strain deformation, Acta Mater. 46 (1998) 5509-5522.

[19] H. Ding, Y. C. Shin, Multi-physics modeling and simulations of surface microstructure alteration in hard turning, J. Mater. Process. Technol. 213 (2013) 877-886.

[20] L. E. Lindgren, Q. Hao, D. Wedberg, Improved and simplified dislocation density based plasticity model for AISI 316 L, Mech. Mater. 108 (2017) 68-76.

[21] R. Liu, M. Salahshoor, S. N. Melkote, T. Maurish, The prediction of machined surface hardness using a new physics-based material model, 2nd CIRP Conference on Surface Integrity (CSI), Procedia Cirp, 13 (2014) 249-256.

[22] A. Chamanfar, M. Jahazi, J. Gholipour, P. Wanjara, S. Yue, Evolution of flow stress and microstructure during isothermal compression of Waspaloy. Mater. Sci. Eng. A, 615 (2014) 497-510.

[23] G. Shen, S. L. Semiatin, R. Shivpuri, Modeling microstructural development during the forging of Waspaloy, Metall. Mater. Trans. A 26 (1995) 1795-1803.

[24] A. Del Prete, L. Filice, D. Umbrello, Numerical simulation of machining nickel-based alloys, Proc. CIRP, 8 (2013) 540-545.

[25] I. S. Jawahir, E. Brinksmeier, R. M'saoubi, D. K. Aspinwall, J. C. Outeiro, D. Meyer, D. Umbrello, A. D. Jayal, Surface integrity in material removal processes: Recent advances. CIRP Ann-Manuf. Technol., 60 (2011) 603-626.

[26] D. Ulutan, T. Ozel, Machining induced surface integrity in titanium and nickel alloys: A review, Int. J. Mach. Tools Manuf. 51 (2011) 250-280.

[27] U.F. Kocks, H. Mecking, Physics and phenomenology of strain hardening: the FCC case, Prog. Mater. Sci., 48 (2003) 171–273.

[28] U. Messerschmidt, Dislocation dynamics during plastic deformation, first ed., Springer-Verlag Berlin, Heidelberg, 2010.

[29] W. S. Lee, C. F. Lin, T. H. Chen, H. W. Chen, Dynamic mechanical behaviour and dislocation substructure evolution of Inconel 718 over wide temperature range, Mater. Sci. Eng. A, 528 (2011) 6279-6286.

[30] H. Ni, A.T. Alpas, Sub-micrometer structures generated during dry machining of copper, Mater. Sci. Eng. A, 361 (2003) 338-349

[31] M. Furukawa, Z. Horita, M. Nemoto, R. Z. Valiev, T. G. Langdon, Microhardness measurements and the Hall-Petch relationship in an Al-Mg alloy with submicrometer grain size, Acta Mater., 44 (1996) 4619-4629.

[32] H. Conrad, The athermal component of the flow stress in crystalline solids, Mater. Sci. Eng. A 6 (1970) 265-273.

[33] E. Arzt, Size effects in materials due to microstructural and dimensional constraints: a comparative review, Acta Mater. 46 (1998) 5611-5626.

[34] O. Takehiro, R. Watanabe, T. Fukui, K. Tanaka, Isothermal Forging of Waspaloy in Air with a New Die Material, Trans. I. S. I. J., 28 (1988) 958-964.

[35] Y. Bergström, A dislocation model for the strain-ageing behaviour of steel, Mater. Sci. Eng. 9 (1972) 101-110.

[36] Y. Bergström, Dislocation model for the stress-strain behaviour of polycrystalline alpha-iron with special emphasis on the variation of the densities of mobile and immobile dislocations, Mater. Sci. Eng. 5 (1969/70) 193-200.

[37] Y. Bergström, The Plastic Deformation of Metals--a Dislocation Model and Its Applicability, Rev. Powder Metall. Phys. Ceram. 2.2 (1983) 79-265.

[38] Y. Estrin, Dislocation theory based constitutive modelling: foundations and applications, J. Mater. Process. Technol. 81 (1998) 33-39.

[39] D. Holt, Dislocation cell formation in metals, J. Appl. Phys. 41 (1970) 3197-3201.

[40] Y. Bergström, H. Hallen, An improved dislocation model for the stress-strain behaviour of polycrystalline [alpha]-Fe, Mater. Sci. Eng. 55 (1982) 49-61.

[41] T. Johnston, C. Feltner, Grain size effects in the strain hardening of polycrystals, Metal. Mater. Trans. B (1970) 1161-1167.

[42] J.C. Li, Petch relation and grain boundary sources. TMS-AIME, 227 (1963) 239.

[43] R. O. Scattergood, C.C. Koch, A modified model for Hall-Petch behavior in nanocrystalline materials, Scripta Metall. Mater. 27 (1992) 1195-1200.

[44] M.A. Meyers, K.K. Chawla, Mechanical Metallurgy: Principles and Applications, Prentice-Hall 1984.

[45] G. J. Thomas, R.W. Siegel, J.A. Eastman, Grain boundaries in nanophase palladium: high resolution electron microscopy and image simulation. Scripta Metall. Mater. 24 (1990) 201-206.

[46] W. Wunderlich, Y. Ishida, R. Maurer, HREM-studies of the microstructure of nanocrystalline palladium. Scripta Metall. Mater. 24 (1990) 403-408.

[47] S. N. Melkote, R. Liu, P. F. Zelaia, T. Marusich, A physically based constitutive model for simulation of segmented chip formation in orthogonal cutting of commercially pure titanium, CIRP Ann-Manuf. Technol., 64 (2015) 65-68.

[48] G. Shen, J. Rollins, D. Furrer, Microstructure modeling of forged Waspaloy discs, Superalloys, 613-620.

[49] D. Caillard, J.L. Martin, Thermally Activated Mechanisms in Crystal Plasticity, Pergamon, Oxford (2003).

[50] H. Frost, M. Ashby, Deformation-mechanism maps - the plasticity and creep of metals and ceramics. Pergamon Press, Oxford, (1982).

[51] H. Ding, Y. C. Shin, Multi-physics modeling and simulations of surface microstructure alteration in hard turning, J. Mater. Process. Technol. 213 (2013) 877-886.

[52] V. P. Astakhov, S. Joksch, Metalworking fluids (MWFs) for cutting and grinding – fundamentals and recent advances, 147–151; first ed., Woodhead Publishing Limited, Cambridge, 2012.

[53] C. Courbon, F. Pusavec, F. Dumont, J. Rech, J. Kopac, Tribological behaviour of Ti6Al4V and Inconel718 under dry and cryogenic conditions-Application to the context of machining with carbide tools, Tribology International 66 (2013) 72–82.

[54] D. Umbrello, Finite element simulation of conventional and high speed machining of Ti6Al4V alloy, J. Mater. Process. Technol. 66, (2013) 72-82.

[55] T. Sakai, A. Belyakov, R. Kaibyshev, H. Miura, J. J. Jonas, Dynamic and post-dynamic recrystallization under hot, cold and severe plastic deformation conditions, Prog. Mater. Sci. 60, (2014) 130-207.

[56] K. Huang, R. E Logé, A review of dynamic recrystallization phenomena in metallic materials, Mater. Des. 111, (2016) 548-574.

[57] G. Krishnamurthy, S. Bhowmick, W. Altenhof, A.T. Alpas, Increasing efficiency of Ti-alloy machining by cryogenic cooling and using ethanol in MRF, CIRP J. Manuf. Sci. and Technol., 18 (2017) 159-172.

[58] J. Schoop, W. F. Sales, I. S. Jawahir, High speed cryogenic finish machining of Ti-6Al4V with polycrystalline diamond tools, J. Mater. Process. Technol., 250 (2017) 1-8.

[59] I. S. Jawahir, H. Attia, D. Biermann, J. Duflou, F. Klocke, D. Meyer, S. T. Newman, F. Pusavech, M. Putz, J. Rech, V. Schulze, D. Umbrello, Cryogenic manufacturing processes, CIRP Ann, 65 (2016) 713-736.

[60] P. Fernandez-Zelaia, S. N. Melkote, Validation of Material Models for Machining Simulation Using Mechanical Properties of the Deformed Chip, Proc-CIRP, 58 (2017) 535-538.

[61] M. Ravi Shankar, S. Chandrasekar, A. H. King, W. D. Compton, Microstructure and stability of nanocrystalline aluminum 6061 created by large strain machining, Acta Mater., 53 (2005) 4781-4793.

[62] M. Ravi Shankar, B. C. Rao, S. Lee, S. Chandrasekar, A. H. King, W. D. Compton, Severe plastic deformation (SPD) of titanium at near-ambient temperature, Acta Mater., 54 (2006) 3691-3700.

[63] C. Reuber, P. Eisenlohr, F. Roters, D. Raabe, Dislocation density distribution around an indent in single-crystalline nickel: Comparing nonlocal crystal plasticity finite-element predictions with experiments, Acta Mater., 71 (2014) 333-348.

Tables and Captions

Table 1: Experimental test conditions.

Cutting Speed [m/min]	**Feed Rate [mm/rev]**	**Cutting Condition**
40	0.05/0.10/0.15	Dry/Wet/Cryogenic
55	0.05/0.10	Dry/Wet/Cryogenic
55	0.15	Wet/Cryogenic
70	0.05/0.10	Dry/Wet/Cryogenic
70	0.15	Wet/Cryogenic

Table 2: Numerical constants identified after the calibration procedure.

Numerical constants	Value	Numerical constants	Value
α	0.35	Q_v [J/mol]	220000

K_c	2.10E+01	D_{v0} [m^2/s]	5.50E-06
Ω_0	10	α^0_G	2.7
Ω_{r0}	0.18	d [$\mu m^{-0.5}$]	1
Δ_{f0}	0.4	ν	1.40E+00
ρ_0 [m^{-2}]	5.00E+11	q	1.34
p	0.27	m	3.06

Table 3: Overall error obtained at the end of the calibration procedure.

	Calibration test		***Friction Coeff.***		***Error %***			***Overall***
	V_c [m/min]	***f [mm/rev]***	***μ***	***m***	***Fc***	***Ft***	***T***	***Absolute Error %***
DRY	40	0.05	0.41	0.37	1.55%	11.81%	-4.18%	5.85%
	40	0.15	0.28	0.40	-1.03%	2.55%	-1.04%	1.54%
	55	0.1	0.31	0.30	6.06%	-2.46%	-0.76%	3.09%
	70	0.1	0.28	0.21	8.69%	18.80%	-5.23%	10.91%
WET	40	0.05	0.08	0.08	-0.87%	4.34%	-3.14%	2.78%
	40	0.15	0.30	0.30	-0.30%	-9.77%	3.46%	4.51%
	55	0.1	0.19	0.19	-2.63%	-0.64%	-3.91%	2.39%
	70	0.1	0.20	0.20	-0.54%	4.83%	-6.72%	4.03%
CRYOGENIC	40	0.05	0.37	0.37	9.08%	1.24%	14.29%	8.20%
	40	0.15	0.27	0.27	2.25%	-3.39%	7.33%	4.32%
	55	0.1	0.28	0.28	-2.29%	3.32%	21.96%	9.19%
	70	0.1	0.24	0.24	9.20%	8.78%	7.25%	8.41%
		Overall Absolute Error %			3.71%	5.99%	6.60%	

Table 4: Overall error obtained at the end of the validation procedure.

	Validation test		***Friction Coeff.***		***Error %***			***Overall Absolute Error %***
	V_c [m/min]	***f [mm/rev]***	***μ***	***m***	***Fc***	***Ft***	***T***	
DRY	40	0.1	0.34	0.39	0.54%	-9.46%	4.13%	4.71%
	55	0.05	0.37	0.28	1.49%	7.23%	-10.38%	6.37%
	70	0.05	0.34	0.20	1.27%	31.89%	-1.91%	11.69%
WET	40	0.1	0.19	0.19	-5.57%	-5.45%	-2.07%	4.36%
	55	0.05	0.08	0.08	1.45%	12.20%	-3.46%	5.70%
	55	0.15	0.30	0.30	3.04%	-15.13%	-5.91%	8.02%
	70	0.05	0.09	0.09	1.82%	16.21%	-8.17%	8.74%
	70	0.15	0.31	0.31	9.10%	2.09%	-6.29%	5.83%
CRYOGENIC	40	0.1	0.32	0.32	18.13	7.03%	19.15%	14.77%
	55	0.05	0.33	0.33	4.44%	7.32%	12.43%	8.06%
	55	0.15	0.23	0.23	-1.26%	-11.51%	4.52%	5.76%
	70	0.05	0.29	0.29	5.09%	7.58%	-6.91%	6.53%
	70	0.15	0.19	0.19	8.68%	-5.50%	5.35%	6.51%
			Overall Absolute Error %		4.76%	9.21%	6.97%	

Figures and Captions

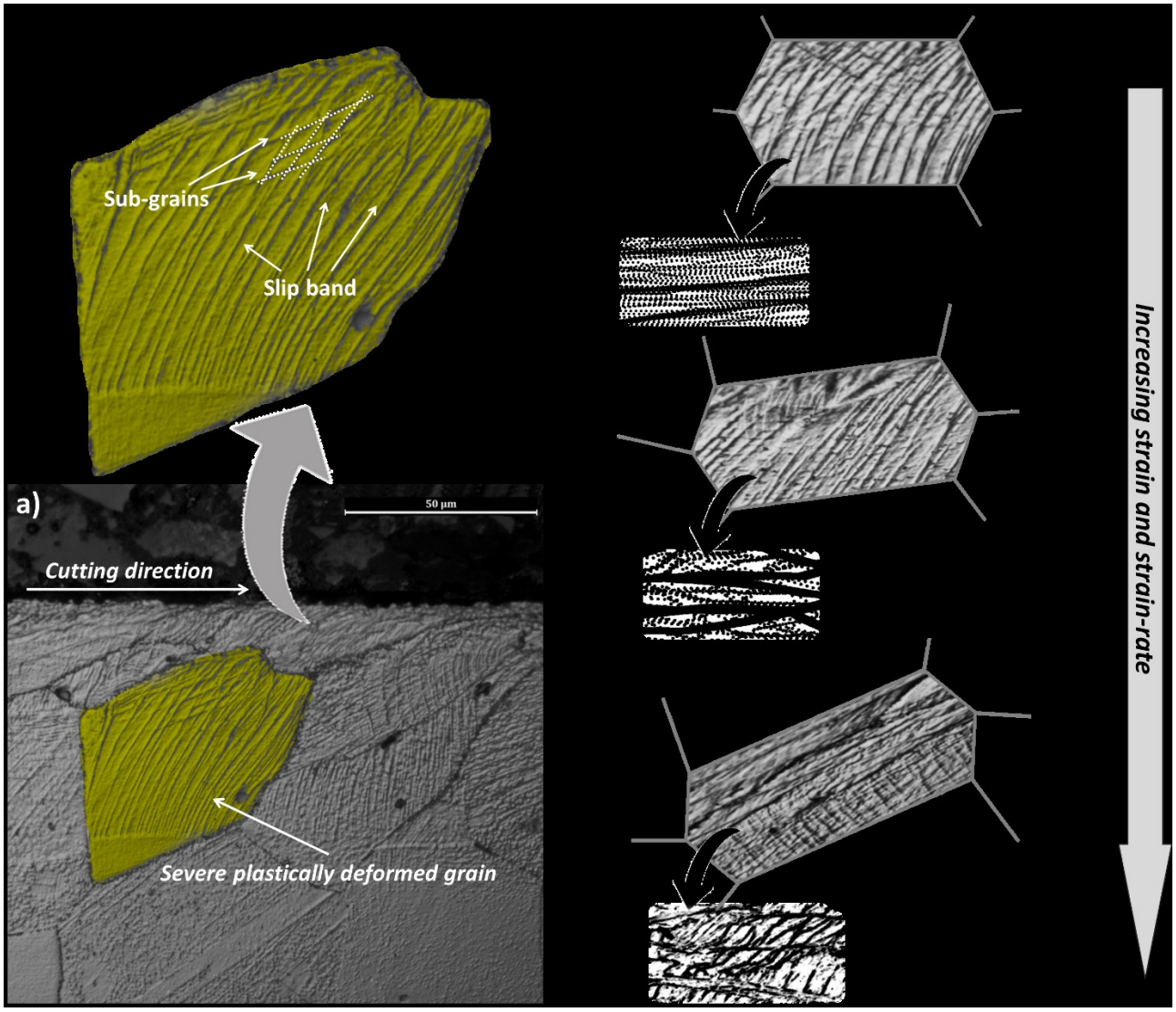

Figure 1. Deformation mechanisms induced on Waspaloy machined surface; a) V_c = 55m/min f = 0.1mm/rev dry condition, b), c) and d) different stages of deformation mechanisms.

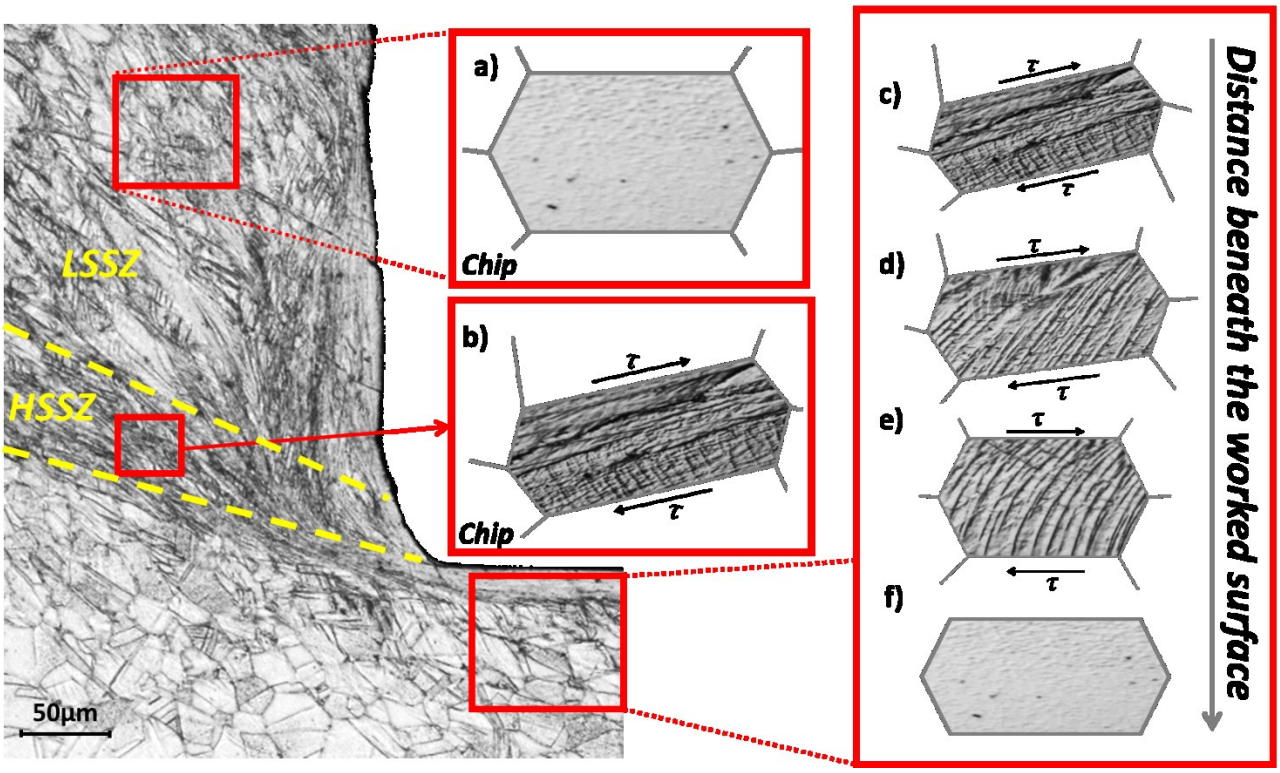

Figure 2: Different deformation mechanisms in chip 1a) and 2a) and in the machined surface 1b), 2b) and 3b)

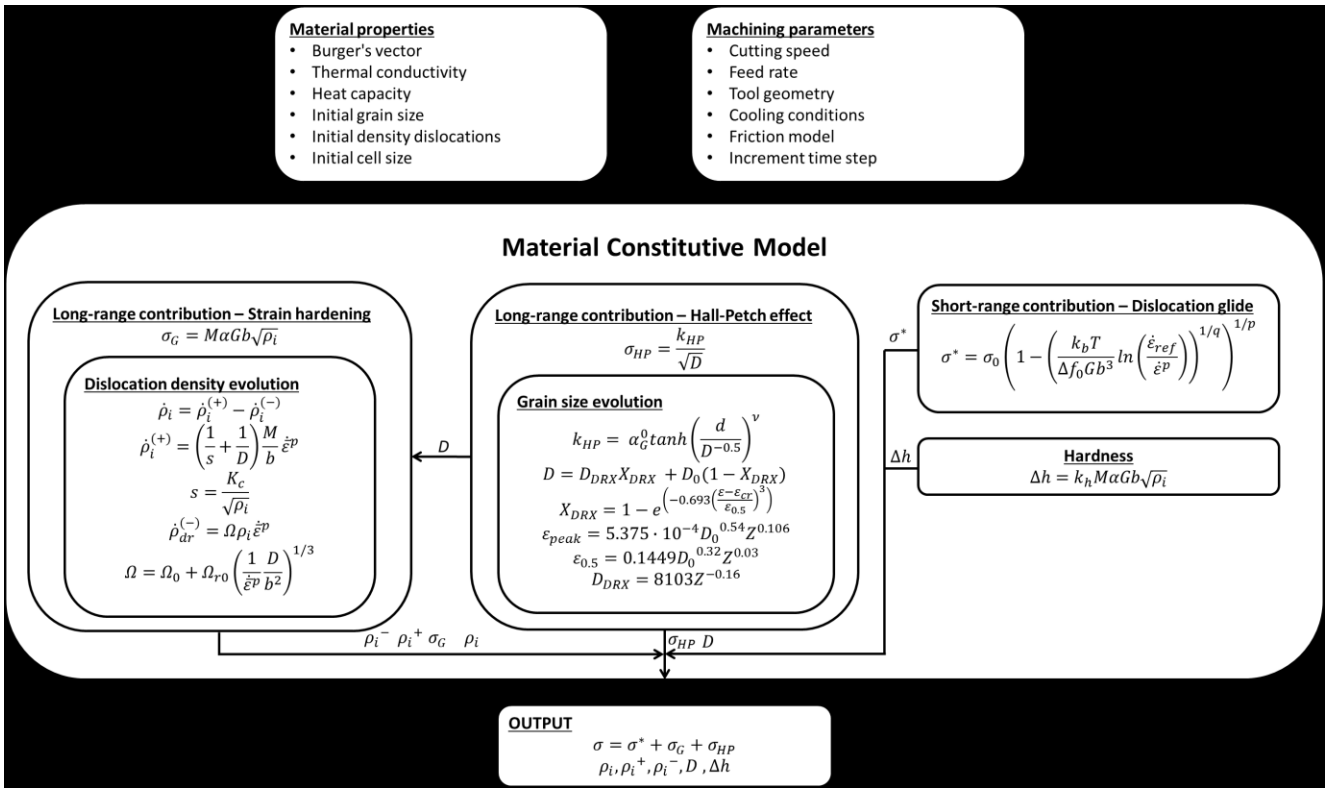

Figure 3: Prediction stategy implemented via sub-routine to simulate the material behavior of the Waspaloy during machining operations.

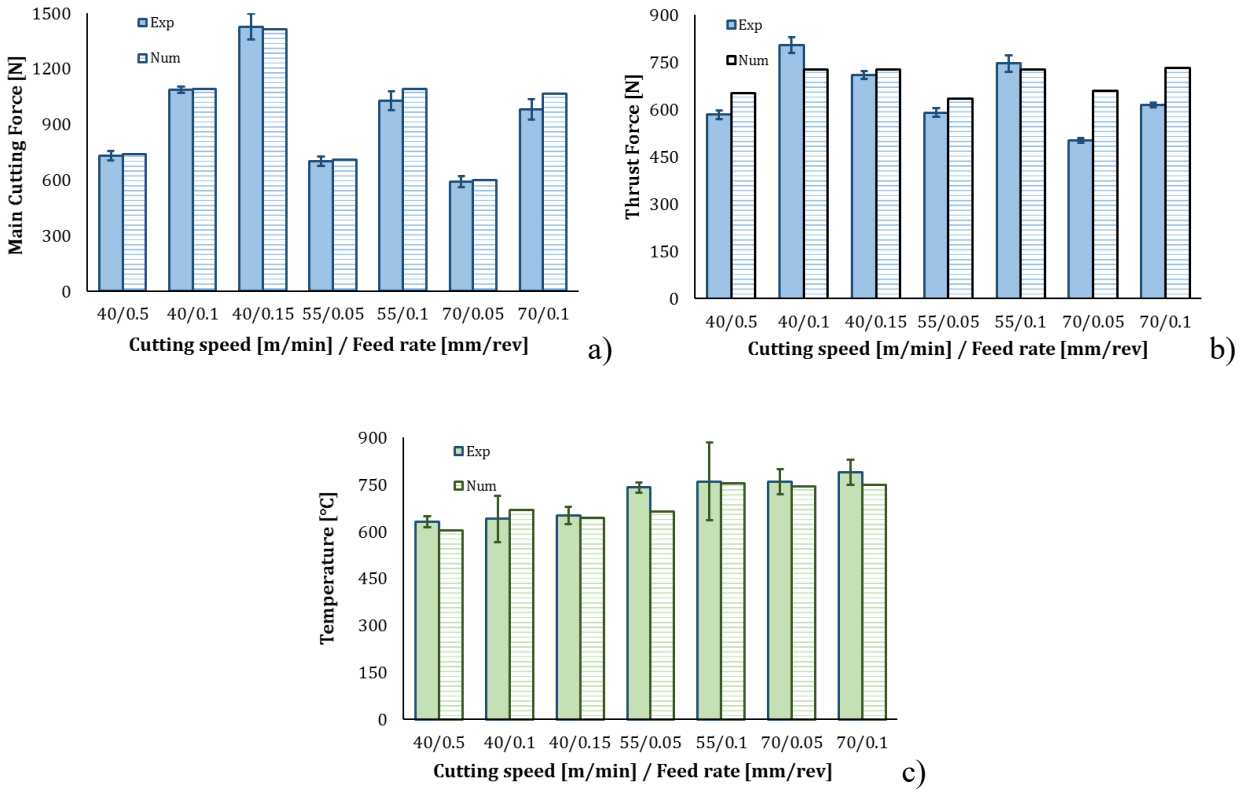

Figure 4: Mean and variation of experimental (EXP) and numerical simulated (NUM) cutting force (a), thrust force (b) and temperatures (c) for different cutting parameters in dry cutting condition.

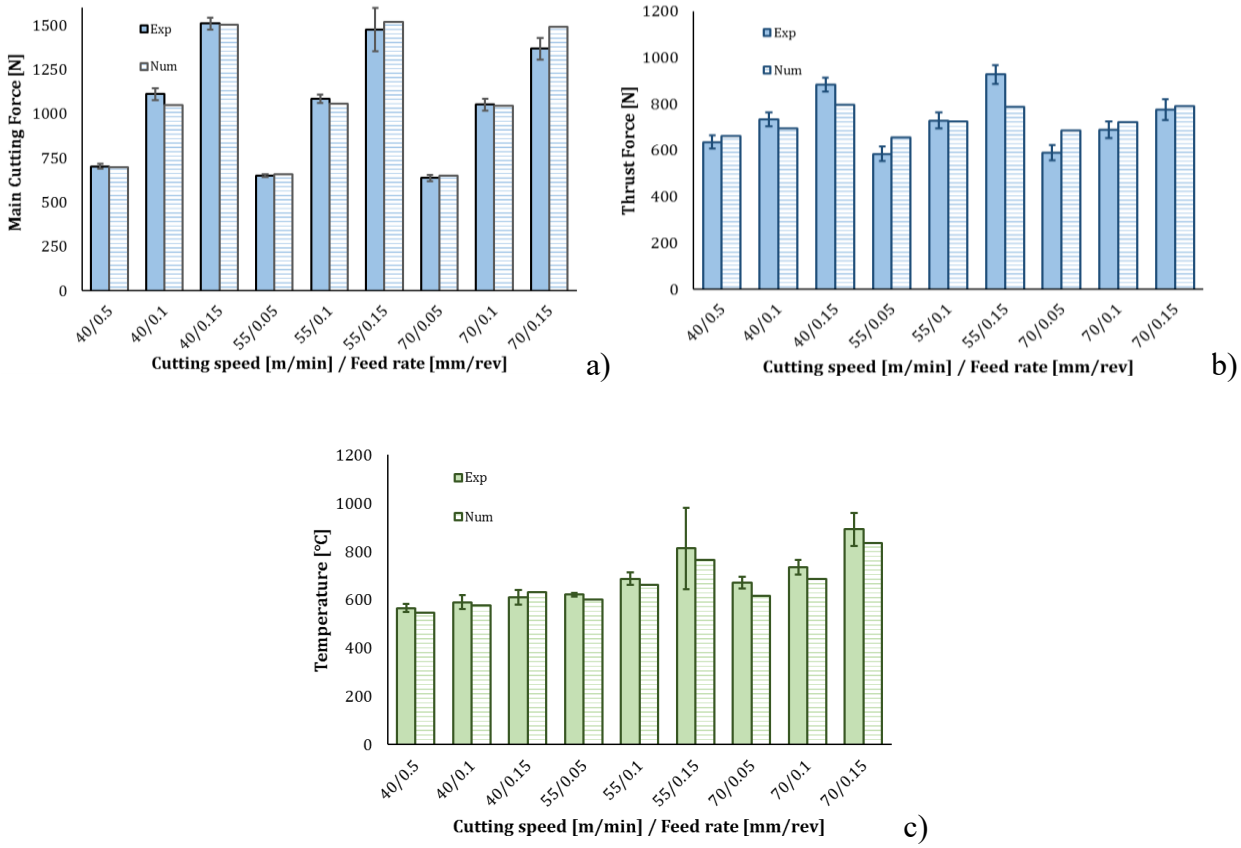

Figure 5: Mean and variation of experimental (EXP) and numerical simulated (NUM) cutting force (a), thrust force (b) and temperatures (c) for different cutting parameters in wet cutting condition.

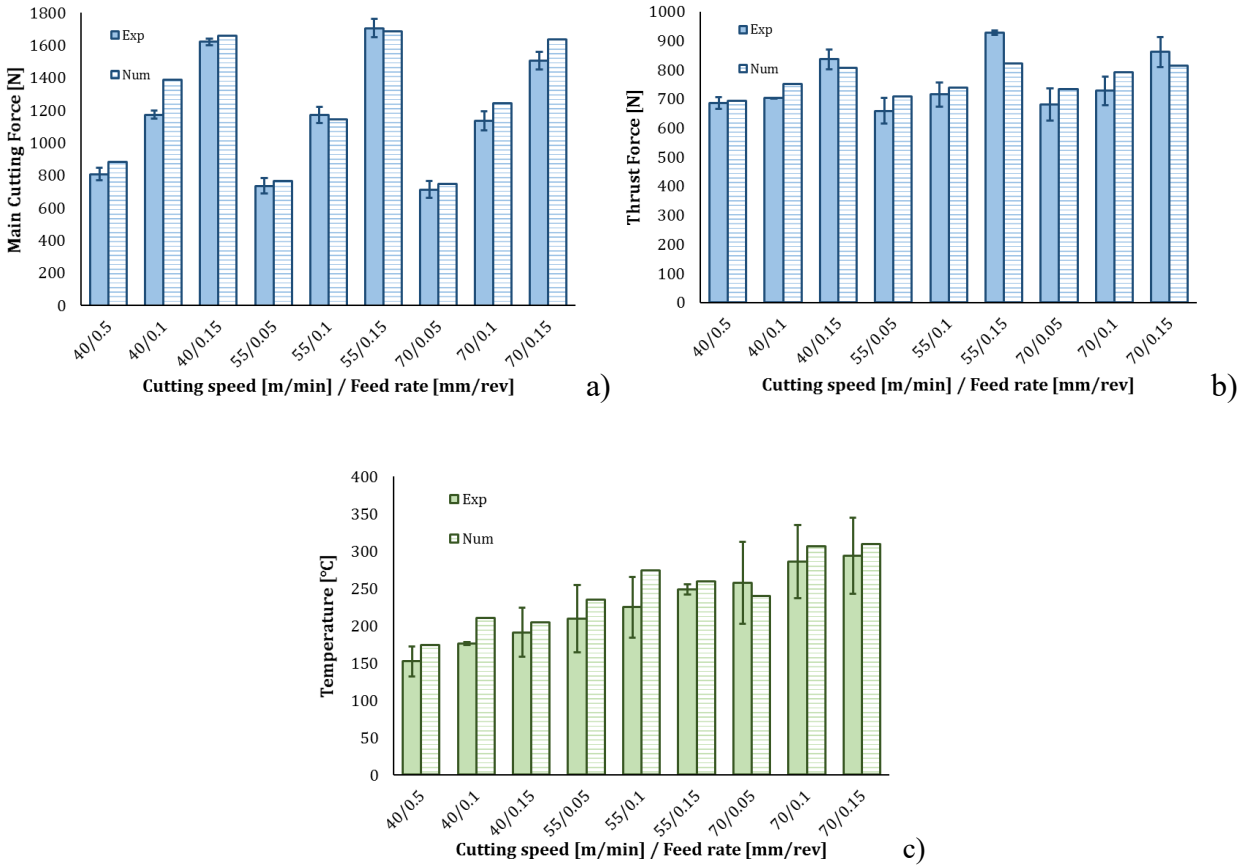

Figure 6: Mean and variation of experimental (EXP) and numerical simulated (NUM) cutting force (a), thrust force (b) and temperatures (c) for different cutting parameters in cryogenic cutting condition.

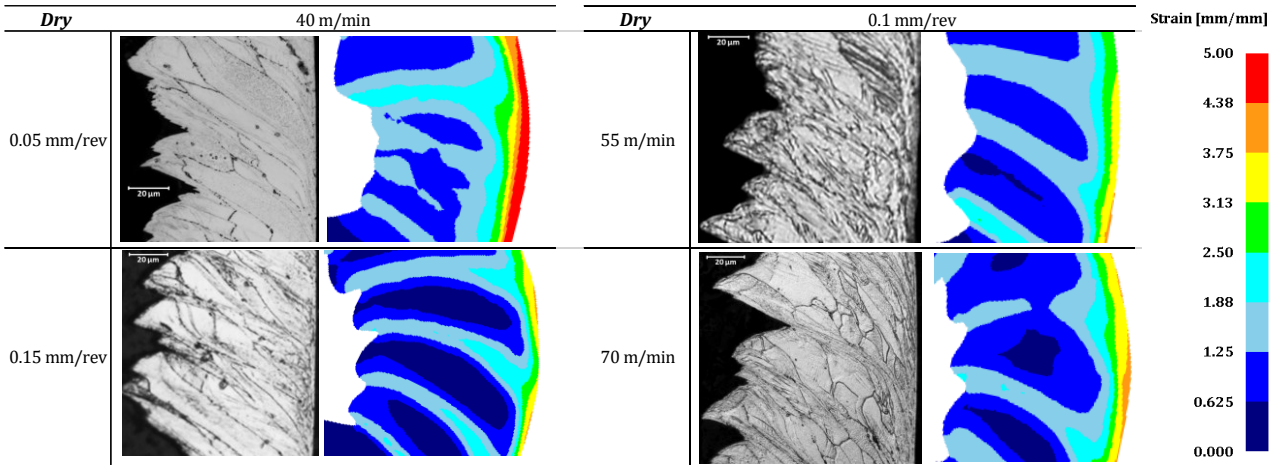

Figure 7: Comparison between experimental and numerical predicted chip formation at different cutting parameters in dry machining condition.

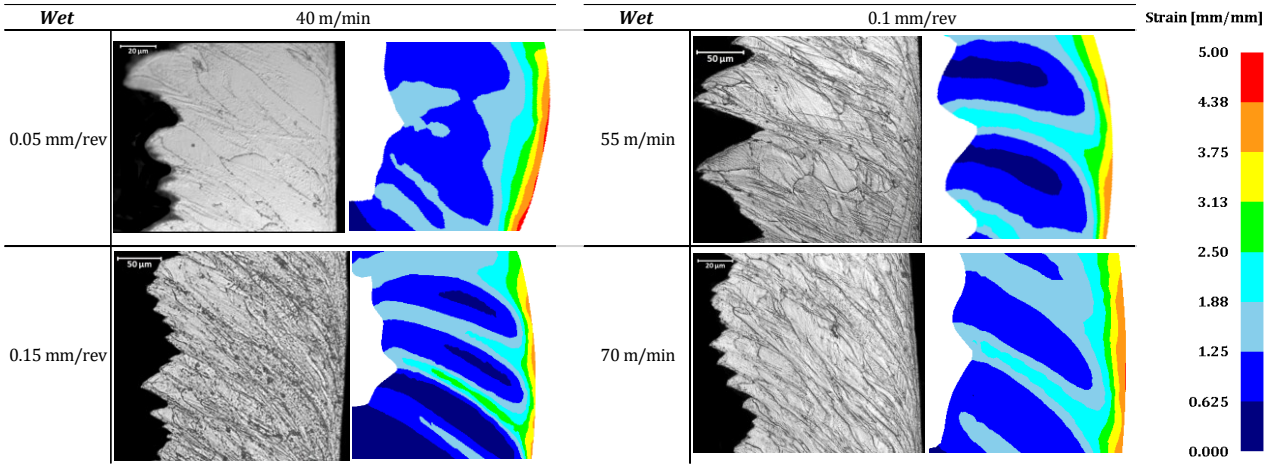

Figure 8: Comparison between experimental and numerical predicted chip formation at different cutting parameters in wet machining condition.

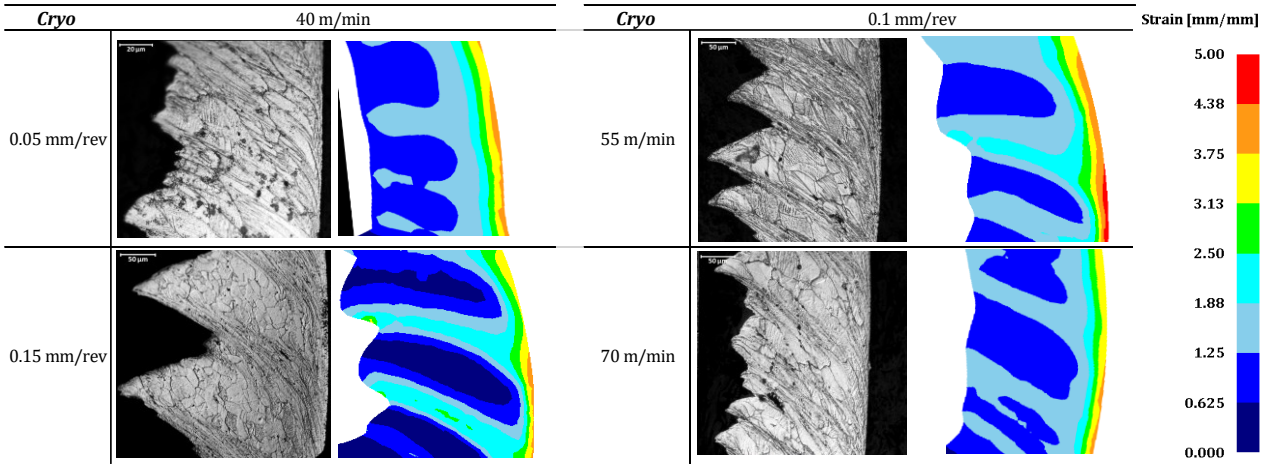

Figure 9: Comparison between experimental and numerical predicted chip formation at different cutting parameters in cryogenic machining condition.

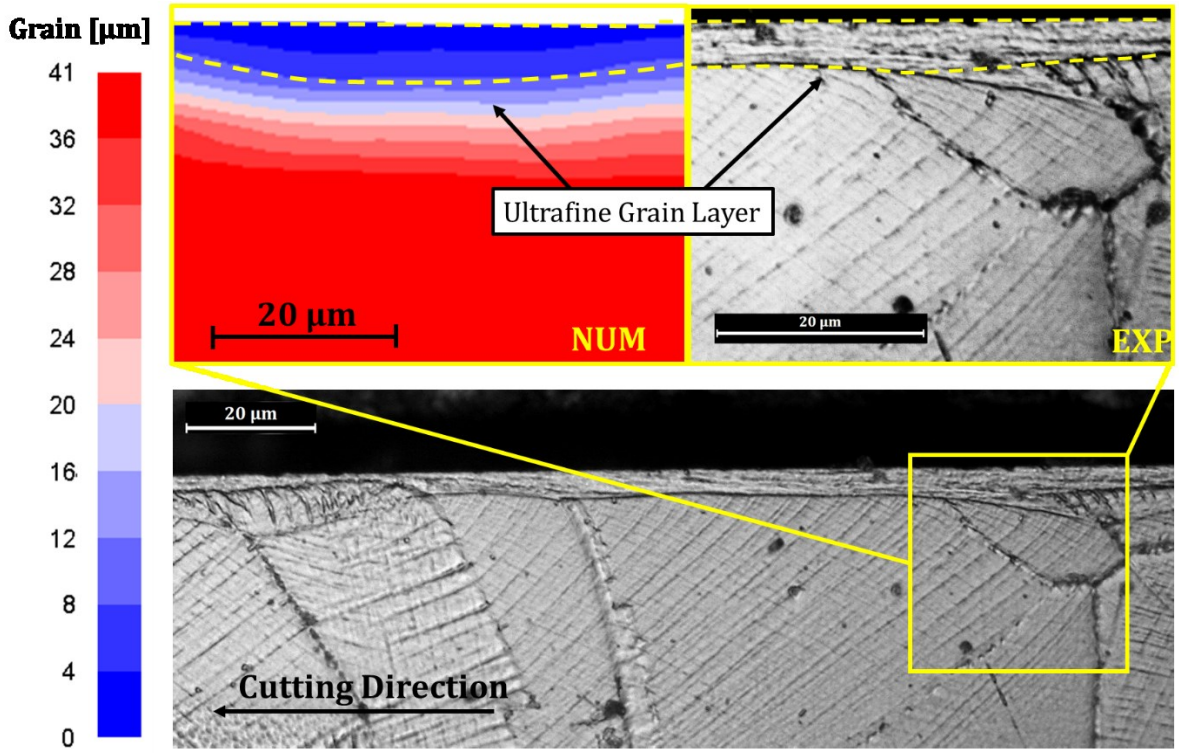

Figure 10: Microstructure prediction and comparison with the micrographs of the machined surface (Vc=70m/min, f=0.1mm/rev, cryogenic condition).

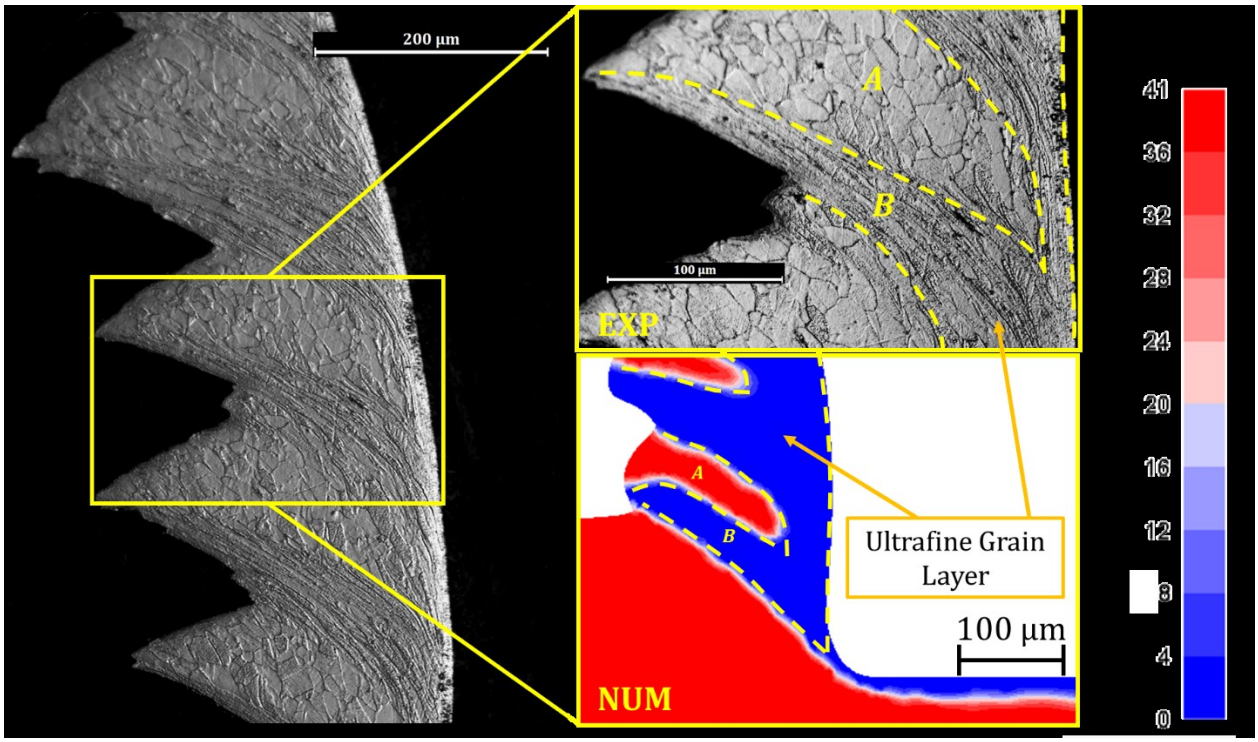

Figure 11: Microstructure prediction and comparison with the micrographs of the machined chip (V_c=70m/min, f=0.1mm/rev, cryogenic condition).

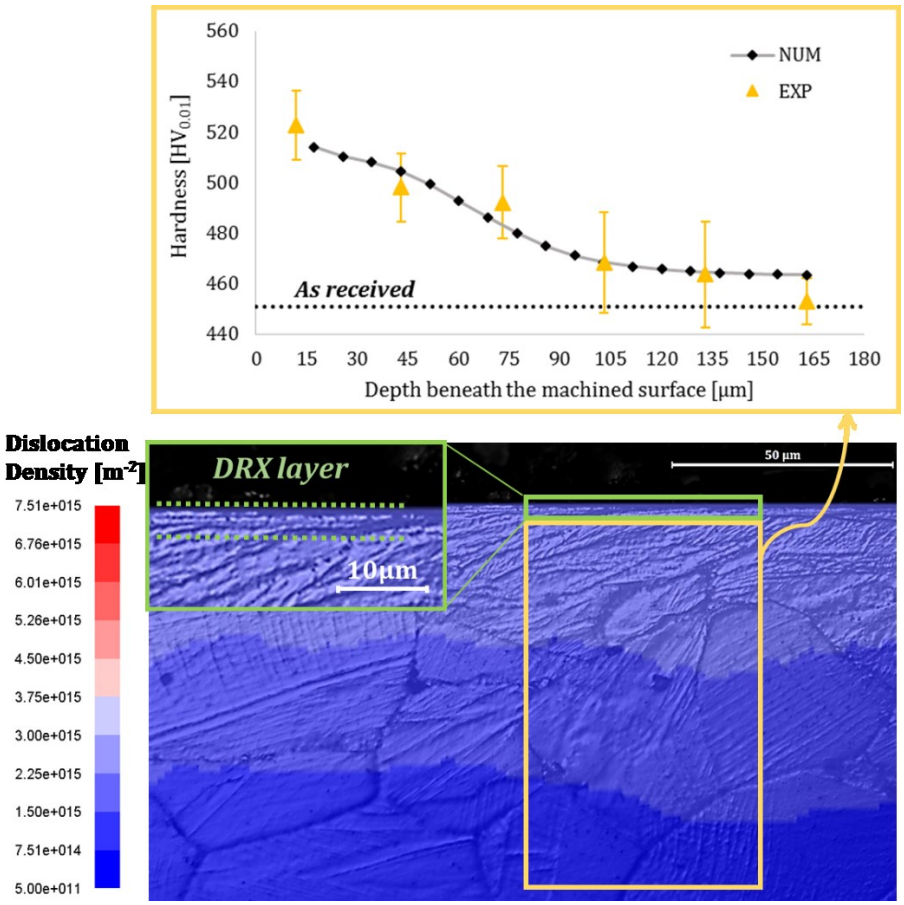

Figure 12: Dislocation concentration beneath the worked surface and consequent hardness variation, V_c=40m/min – f=0.15mm/rev – cryogenic. (the dislocation density prediction is superposed to the optical micrograph).

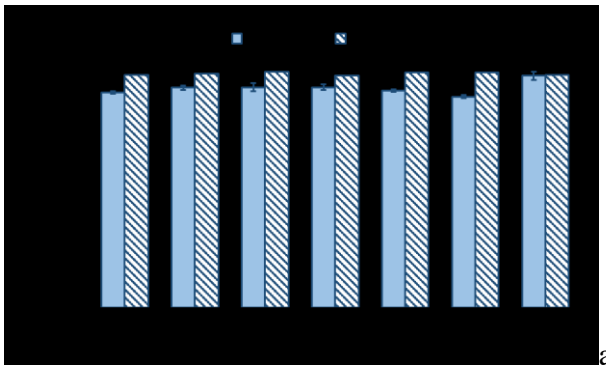
a)
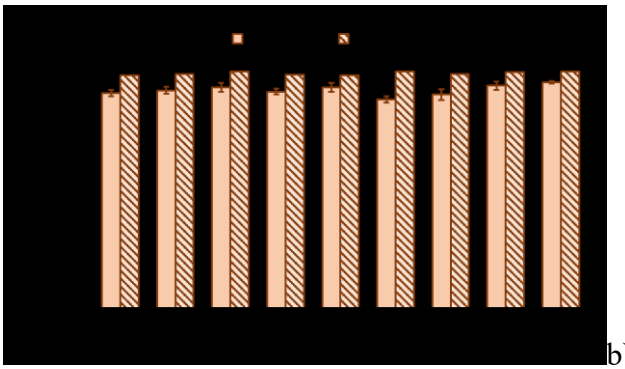
b)
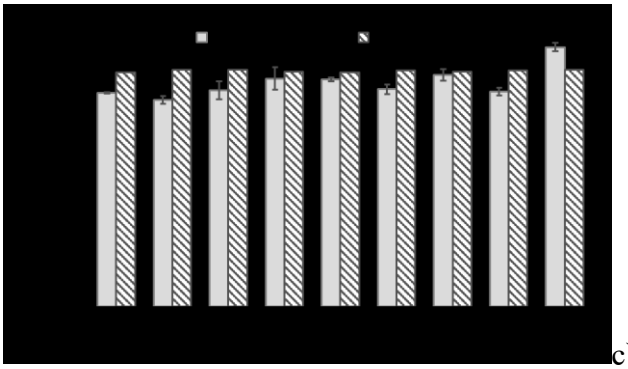
c)

Figure 13: Mean and variation of experimental (EXP) and numerical simulated (NUM) hardness beneath the worked surface in dry (a), wet (b) and cryogenic (c) machining conditions.

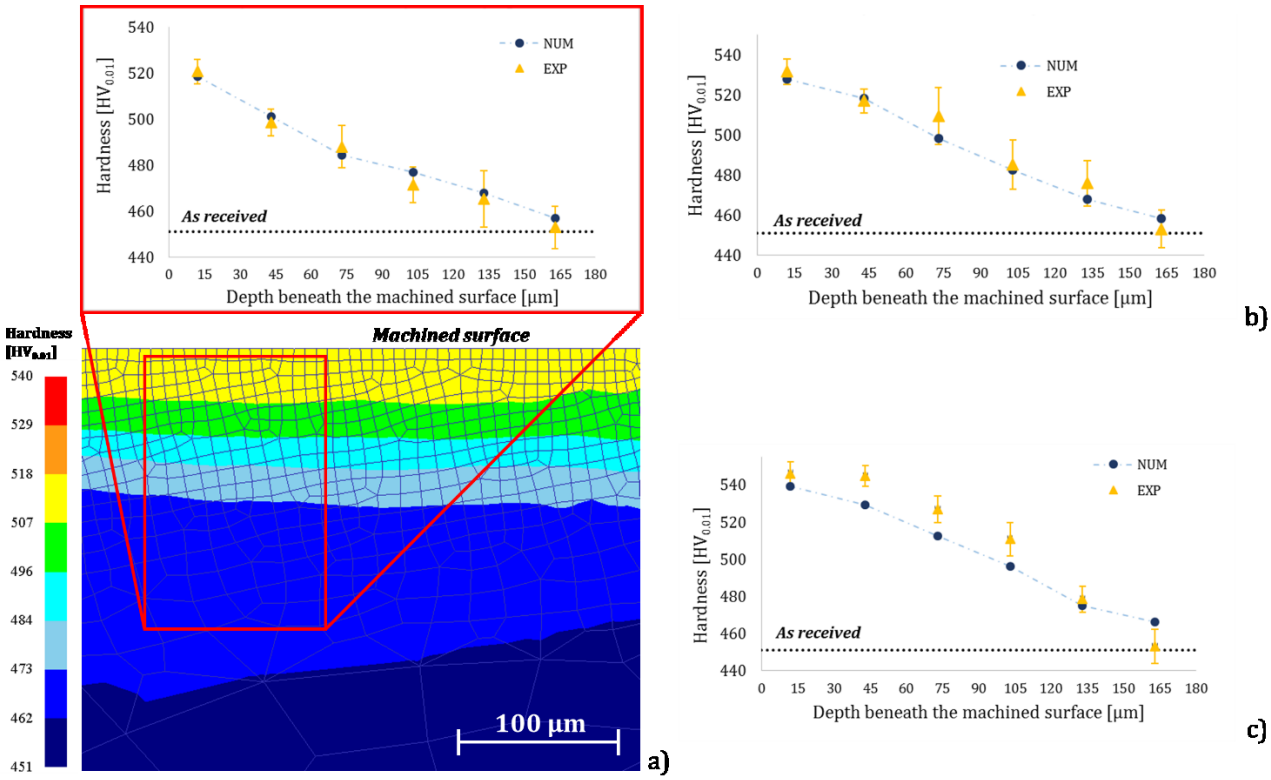

Figure 14: Comparison between the experimental (EXP) and numerical simulated (NUM) hardness through the affected layer in cryogenic (a), wet (b) and dry (c) cooling conditions at V_c=70m/min – f=0.1mm/rev.

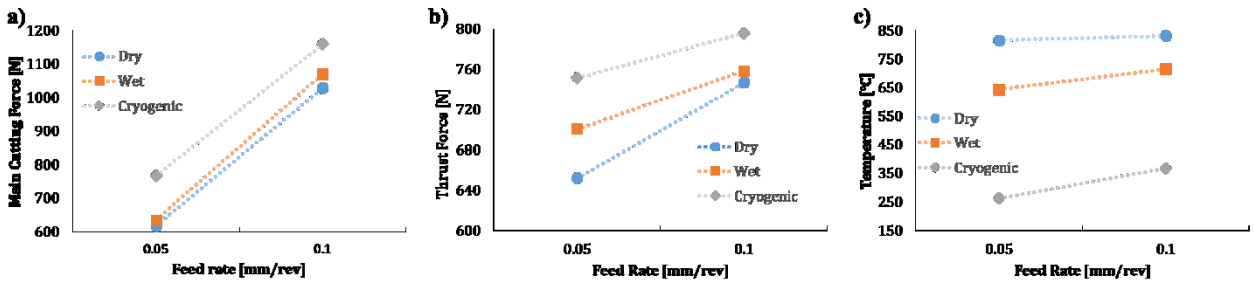

Figure 15: a) Main Cutting Force; 9b) Thrust Force; c) Temperature at cutting speed of 85m/min varying cutting conditions.

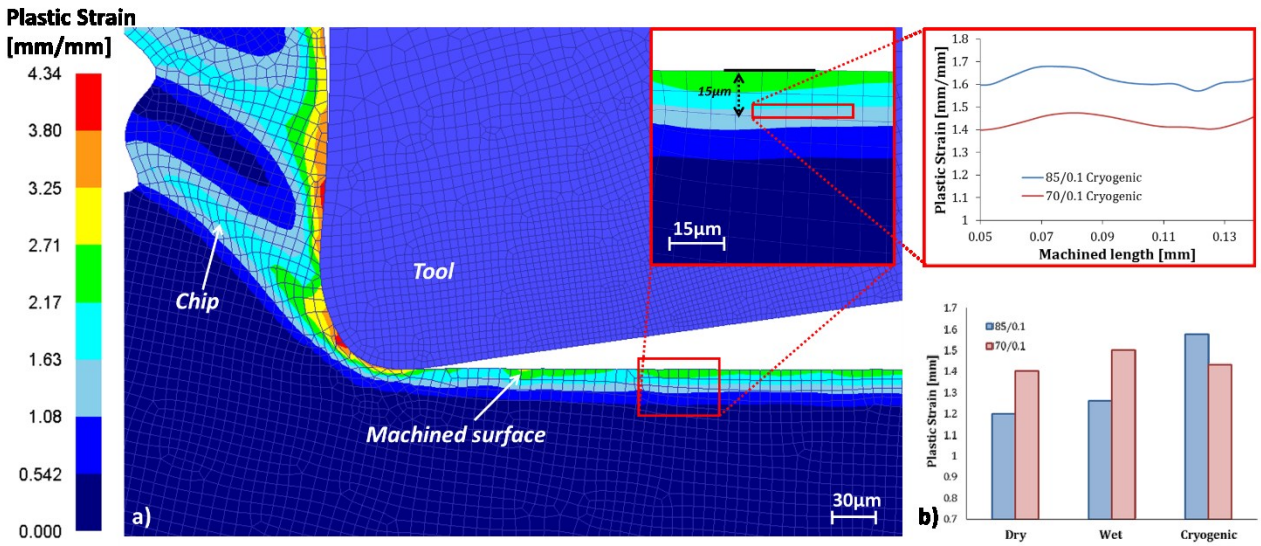

Figure 16: Predicted plastic strain a) at cutting speed of 85m/min, feed rate of 0.1mm/rev under cryogenic conditions; b) average value of plastic deformation at different cooling conditions.

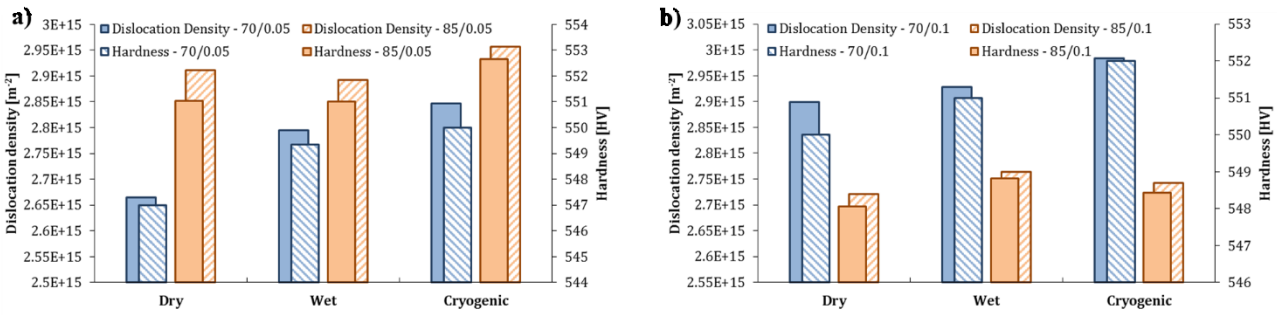

Figure 17: Computed average value of dislocation density and hardness at varying cutting speed (70m/min and 85m/min), feed rate (0.05mm/rev and 0.1mm/rev) and cooling conditions. (METTERE STESSA SCALA SIA PER DENSITA' CHE PER HV!!!!)